The Astrophysical Journal, 854:3 (8pp), 2018 February 10 https://doi.org/10.3847/1538-4357/aaa70f


# Decrease in Hysteresis of Planetary Climate for Planets with Long Solar Days

Dorian S. Abbot, Jonah Bloch-Johnson, Jade Checlair, Navah X. Farahat,
R. J. Graham, David Plotkin, Predrag Popovic, and Francisco Spaulding-Astudillo
Department of the Geophysical Sciences, University of Chicago, 5734 South Ellis Avenue, Chicago, IL 60637, USA; abbot@uchicago.edu
*Received 2017 November 21; revised 2017 December 30; accepted 2018 January 9; published 2018 February 6*

## Abstract

The ice-albedo feedback on rapidly rotating terrestrial planets in the habitable zone can lead to abrupt transitions (bifurcations) between a warm and a snowball (ice-covered) state, bistability between these states, and hysteresis in planetary climate. This is important for planetary habitability because snowball events may trigger rises in the complexity of life, but could also endanger complex life that already exists. Recent work has shown that planets tidally locked in synchronous rotation states will transition smoothly into the snowball state rather than experiencing bifurcations. Here we investigate the structure of snowball bifurcations on planets that are tidally influenced, but not synchronously rotating, so that they experience long solar days. We use PlaSIM, an intermediate-complexity global climate model, with a thermodynamic mixed layer ocean and the Sun's spectrum. We find that the amount of hysteresis (the range in stellar flux for which there is bistability in climate) is significantly reduced for solar days with lengths of tens of Earth days, and disappears for solar days of hundreds of Earth days. These results suggest that tidally influenced planets orbiting M and K stars that are not synchronously rotating could have much less hysteresis associated with the snowball bifurcations than they would if they were rapidly rotating. This implies that the amount of time it takes them to escape a snowball state via $CO_2$ outgassing would be greatly reduced, as would the period of cycling between the warm and snowball state if they have low $CO_2$ outgassing rates.

*Key words:* astrobiology – planets and satellites: atmospheres

## 1. Introduction

Earth has experienced a few episodes of global, or very near-global, ice coverage that are called "snowball Earth" events (Kirschvink 1992; Hoffman et al. 1998). These events may have been critical for increasing the complexity of life, both directly through forcing evolutionary innovations (Kirschvink 1992; Hoffman et al. 1998; Hoffman & Schrag 2002) and indirectly by increasing atmospheric oxygen (Hoffman & Schrag 2002; Laakso & Schrag 2014, 2017). The snowball events on Earth were isolated and lasted for millions to tens of millions of years (Rooney et al. 2015). Habitable zone exoplanets with low $CO_2$ outgassing rates, however, could experience perpetual cycling between snowball and warm states, with most of the time spent in snowball conditions (Tajika 2007; Kadoya & Tajika 2014; Menou 2015; Abbot 2016; Batalha et al. 2016; Haqq-Misra et al. 2016; Paradise & Menou 2017). Understanding how snowball episodes might function on Earth-like exoplanets is therefore critical for planetary habitability.

The ice-albedo feedback occurs when cooling causes the replacement of low-albedo ocean with high-albedo ice, which leads to more cooling and ice formation. As a result of the ice-albedo feedback, rapidly rotating planets exhibit a bifurcation, or jump, in climate, into and out of snowball events (Budyko 1969; Sellers 1969). These bifurcations are associated with bistability for a range of radiative forcing, as well as hysteresis. This is shown schematically in Figure 1. If we start in the warm state and decrease the stellar flux (or equivalently $CO_2$), eventually the climate transitions into the snowball state through a bifurcation at some critical value of the stellar flux. We will refer to this process as the "warm-to-snowball transition." If we then increase the stellar flux, the climate remains in the snowball state even at stellar fluxes where it was previously in the warm state, which reflects the bistability of the system. The "snowball-to-warm transition" occurs when the stellar flux is increased enough for a planet in the snowball state to jump into the warm state. The path dependence of the system that results from bistability is referred to as hysteresis. We can quantify the amount of hysteresis in the system through the range of stellar flux over which the planet is bistable ($\Delta S$) and the difference between the warm and snowball states through the increase in global mean surface temperature associated with the snowball-to-warm transition ($\Delta T$) (Figure 1).

Tidal locking, including into a synchronous 1:1 spin–orbit state, should be common for planets in the habitable zones of the many M and K stars in the solar neighborhood that will be prime targets for future observational missions (Kasting et al. 1993; Barnes 2016). For this reason, Checlair et al. (2017) investigated the effect of synchronous tidal locking on the snowball state. They used PlaSim, an intermediate-complexity global climate model (GCM), to show that planets in synchronous rotation states are unlikely to experience bifurcations and hysteresis associated with the snowball state. Instead, they should transition smoothly from the warm to the snowball state. Checlair et al. (2017) explained the loss of the snowball bifurcation as resulting directly from the change in the pattern of incoming radiation from the central star, in particular, the strong increase in incoming radiation as the substellar point is approached. The loss of hysteresis in planetary climate is important because it means that a synchronously rotating planet with an active carbon cycle (Walker et al. 1981) could not remain in a snowball state. If such a planet happened into a snowball state, weathering would be greatly reduced or zero, and without hysteresis volcanic outgassing of $CO_2$ would immediately warm the planet enough to expose the open ocean at the substellar point.

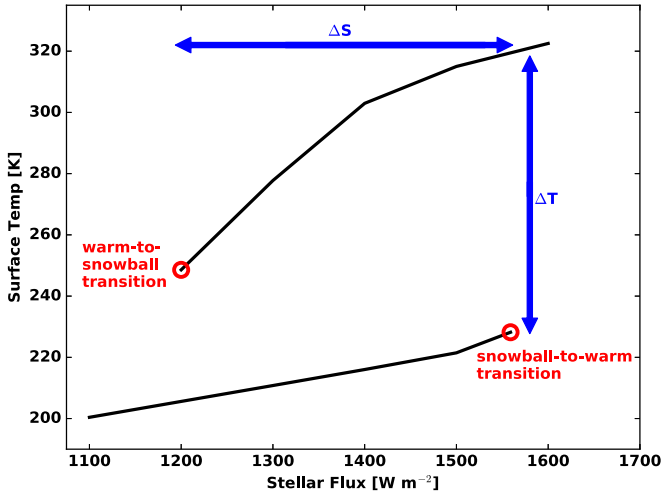


**Figure 1.** This is a plot of a closed hysteresis loop over the allowable states of global mean surface temperature as a function of stellar flux for an idealized rapidly rotating planet (black lines). The two bifurcations in the system are represented by red circles and labeled "warm-to-snowball transition" and "snowball-to-warm transition." The range of stellar flux over which the planet is bistable ($\Delta S$) and the increase in global mean surface temperature associated with the snowball-to-warm transition ($\Delta T$) are represented by blue double arrows.

Tidally influenced planets will not all be synchronously rotating. For high enough eccentricities, they will be caught in higher order spin states (Barnes 2016) and even in a circular orbit they can avoid synchronous rotation because of atmospheric tides (Leconte et al. 2015). This raises the question of what happens to the snowball bifurcation on a planet that is not synchronously rotating, but has a very long solar day (the time from local noon to the next local noon). Boschi & Lucarini (2013) and Lucarini et al. (2013) did some simulations to investigate this using PlaSim with no continents, an ocean with a depth of 50 m, and no ocean heat transport, and found that hysteresis is lost for planets with a solar day greater than about 180 Earth days. In a related study, Salameh et al. (2017) investigated the stellar flux that leads to global glaciation as a function of planetary rotation rate using ECHAM6, a more sophisticated atmospheric GCM. They found that decreasing the rotation rate has a complicated, non-monotonic effect on the stellar flux at which the transition to global glacation occurs, with the transition ultimately occurring at a much lower stellar flux for a synchronously rotating planet.

The purpose of this paper is to study in more depth the transition from a planet with a snowball bifurcation and hysteresis for a short solar day to one without them for a long solar day. We will be particularly interested in determining the critical solar day length at which this change in behavior occurs, understanding in detail what physically leads to this transition, and outlining the implications for planets that will be observable in the near future. In order to isolate the effect of the solar day, we will not consider changes in the planetary rotation rate (Salameh et al. 2017) or the reduction in the ice-albedo feedback for redder stars (Joshi & Haberle 2012; Shields et al. 2013, 2014).

We will use the intermediate complexity GCM PlaSim in this study, run with no continents and a thermodynamic mixed layer ocean with no heat transport and a fixed depth. This model has a lower resolution and somewhat less sophisticated physical parameterizations than the GCMs used to forecast climate change. Its main advantage is that it is numerically efficient so that we can perform a large number of simulations to accurately determine the locations of bifurcations in a variety of situations. More complex 3D atmospheric GCMs (Abbot & Pierrehumbert 2010; Abbot et al. 2012, 2013; Voigt et al. 2012; Voigt 2013; Leconte et al. 2013b, 2013a; Shields et al. 2013, 2014; Yang et al. 2013; Wolf & Toon 2014, 2015; Yang et al. 2014; Way et al. 2015; Kopparapu et al. 2016; Haqq-Misra et al. 2017; Salameh et al. 2017; Wolf 2017; Wolf et al. 2017) and models that include ocean (Voigt et al. 2011; Voigt & Abbot 2012; Yang et al. 2012a, 2012b, 2012c; Hu & Yang 2014; Way et al. 2015; Cullum et al. 2016) and ice dynamics (Goodman & Pierrehumbert 2003; Pollard & Kasting 2005; Goodman 2006; Li & Pierrehumbert 2011; Tziperman et al. 2012; Abbot et al. 2013; Pollard et al. 2017) have been applied to snowball and exoplanet climate before. It will be important to check our results with models including more processes in the future, insofar as this is possible given numerical constraints. Nevertheless, this work is an important first step and outlines physical processes that are likely to be active even in these more sophisticated models.

## 2. Methods

### 2.1. Model

We use PlaSim (Fraedrich et al. 2005), the same intermediate-complexity 3D global climate model (GCM) used by Checlair et al. (2017); Boschi & Lucarini (2013), and Lucarini et al. (2013). PlaSim solves the primitive equations for atmospheric dynamics and has schemes to calculate radiative transfer, convection and clouds, thermodynamic sea ice, and land-atmosphere interactions. We run the model at T21 horizontal resolution (5°.625 × 5°.625) with 10 vertical levels. We use the modern solar spectral distribution, so we do not take into account the stellar effect on the ice-albedo feedback (Joshi & Haberle 2012; Shields et al. 2013, 2014). We use an atmospheric $CO_2$ of 360 ppm and set other trace greenhouse gases to zero. PlaSim calculates $H_2O$ prognostically and includes its radiative effects. The surface boundary is a thermodynamic mixed layer (slab) ocean with zero imposed ocean heat transport and a mixed layer depth that we vary. A mixed layer ocean is essentially a motionless layer of water that provides the surface with a heat capacity proportional to its depth. We use an aquaplanet configuration, with no continents. We set the eccentricity and obliquity to zero.

We use the same basic methodology as Checlair et al. (2017). We first perform simulations to obtain equilibrated climates where the surface is either ice-free (henceforth warm start) or 100% ice-covered (henceforth cold start). For a particular parameter choice, we run simulations starting from both warm and cold starts at a variety of different stellar fluxes. We then use a bisection algorithm to find the stellar fluxes at which bifurcations occur to within 0.5 W m$^{-2}$. We run all simulations until they reach top-of-atmosphere and surface energy balance, typically 60–100 Earth years. We average all displayed variables over 10 Earth years after a simulation has converged. We also performed test simulations along the warm branch of solutions in which we decreased the stellar flux in successive increments of 5 W m$^{-2}$ for each simulation and restarted from the previous converged simulation. We obtained the same results using this method as we did using the standard warm start methodology.

### 2.2. Changing the Solar Day

Following Boschi & Lucarini (2013) and Lucarini et al. (2013), we consider longer solar days by decreasing the length of the year while keeping the planetary rotation rate fixed. This section describes how we modified the radiation scheme to accomplish this.

$T_{\rm orb}$, the orbital period, is the amount of time it takes the planet to orbit its star. The sidereal day, $T_{\rm sid}$, is the amount of time it takes for the planet to do one rotation around its own axis relative to the distant stars. This means that the number of rotations per orbital period is

$$N_{\rm sid} = \frac{T_{\rm orb}}{T_{\rm sid}}. \quad (1)$$

We will take the sidereal day to be constant, but allow $N_{\rm sid}$ to change. The solar day, $T_{\rm sol}$, is the amount of time from local noon to the next local noon on the planet's surface. The number of solar days per orbital period is

$$N_{\rm sol} = \frac{T_{\rm orb}}{T_{\rm sol}}. \quad (2)$$

For a prograde orbit, we must have

$$N_{\rm sid} = 1 + N_{\rm sol}, \quad (3)$$

because the planet orbiting once around the central star cancels out one solar day that the planet would have experienced due to rotation alone. Finally, we define $\theta$ as the longitude of the planet where the central star is directly overhead in radians. Assuming a constant planetary rotation rate and constant motion of the planet around the star (a circular orbit), we find that

$$\theta = 2\pi\frac{t}{T_{\rm sol}}, \quad (4)$$

where $t$ is the time, which we will keep track of in Earth minutes (60 seconds).

Now let us suppose that we wish to consistently change $T_{\rm orb}$ and $T_{\rm sol}$, while keeping $T_{\rm sid}$ constant. Suppose that we want to consider a low-order orbital resonance. In this case $N_{\rm sid}$ defines the resonance, so that, for example, if we consider a 2:1 spin–orbit resonance, $N_{\rm sid} = 2$. Given that we are keeping the rotation rate (and therefore $T_{\rm sid}$) constant, this would mean a very short orbital period. We can solve Equations (1)–(3) for the solar day as follows

$$T_{\rm sol} = T_{\rm sid}\frac{N_{\rm sid}}{N_{\rm sid} - 1} = \frac{T_{\rm orb}}{N_{\rm sid} - 1}. \quad (5)$$

Now we can combine Equations (4) and (5) to solve for $\theta$

$$\theta = 2\pi\frac{t}{T_{\rm orb}}(N_{\rm sid} - 1) = 2\pi\frac{t}{T_{\rm sid}}\frac{N_{\rm sid} - 1}{N_{\rm sid}}, \quad (6)$$

where it is useful to write $\theta$ this way since we are assuming that $T_{\rm sid}$ is constant. Now, let us suppose that the planet we are considering originally, before we change $T_{\rm orb}$, is an idealized version of modern Earth with an orbital period of 360 solar days, each lasting $24 \times 60 = 1440$ minutes. This means the planet has 361 sidereal days, so that

$$T_{\rm sid} = \frac{360}{361}(1440 \text{ minutes}). \quad (7)$$

We are taking $T_{\rm sid}$ to be constant, so we can substitute Equation (7) into Equation (6) and find that

$$\theta = 2\pi\frac{t}{(1440 \text{ minutes})}\frac{361}{360}\frac{N_{\rm sid} - 1}{N_{\rm sid}}. \quad (8)$$

The radiative scheme in PlaSim uses $\theta$ directly, so we can now specify the position of the central star for different values of $N_{\rm sid}$ to the code. Using Equation (5), this is equivalent to specifying the position of the central star for different values of $T_{\rm sol}$.

Before proceeding, let us consider the asymptotic limits of Equation (8). If the planet is tidally locked, then $N_{\rm sid} = 1$, so that by Equation (5), $T_{\rm sol}$ is infinite. In other words, the central star stays above the same place on the planet, as expected. Equation (8) shows that $\theta = 0$ for all times in this limit, which is consistent with tidal locking. Next apply Equation (8) to the original, idealized version of modern Earth. In this case, $N_{\rm sid} = 361$ so that

$$\theta = 2\pi\frac{t}{(1440 \text{ minutes})}. \quad (9)$$

Since $T_{\rm sol} = 1440$ min, in this case, we have recovered our definition of $\theta$.

## 3. Results

For a solar day of 1.99 Earth days and an ocean mixed layer depth of 50 m, we reproduce the familiar Earth-like bifurcation diagram of climate (Figure 2) with two separate climate states that are bistable for a range of stellar flux as a result of the ice-albedo feedback (Budyko 1969; Sellers 1969). The "warm" state has large regions of open ocean and exists for global mean surface temperatures above about 250 K. The "snowball" state is globally ice-covered and exists for global mean surface temperatures below about 225 K. There is also a nearly, but not completely, ice-covered state that occurs close to the transition to global ice coverage (Figure 2). This is similar to states discussed by Abbot et al. (2011) and Rose (2015), but must be associated with a different mechanism than those authors discussed since PlaSim uses the same albedo for snow and bare sea ice and since we use a slab ocean with no ocean heat transport. This state is associated with some hysteresis and may be considered a distinct state; however, it does not appear in most scenarios that we consider and we will simply consider it to be the extreme branch of the warm state for the purposes of this paper.

When we increase the solar day to 360 Earth days, we find that the bifurcations in global climate associated with the ice-albedo feedback disappear (Figure 2), just as Checlair et al. (2017) found for the synchronously rotating case. For this longer solar day, the climate smoothly transitions to global ice coverage. The ice-albedo feedback can still be seen through the increase in the slope of the global mean surface temperature when the planet is partially ice-covered (Figure 2), but it is not strong enough to lead to hysteresis and bistability. In a few cases, some small differences between the equilibrated climate of the warm and cold start simulations persist. Checlair et al. (2017) found that these small differences actually represent a continuum of states allowed by the fact that the sea ice scheme only allows 100% ice-covered or ice-free gridboxes, and that they are not associated with the standard, global ice-albedo feedback (Budyko 1969; Sellers 1969). We can therefore

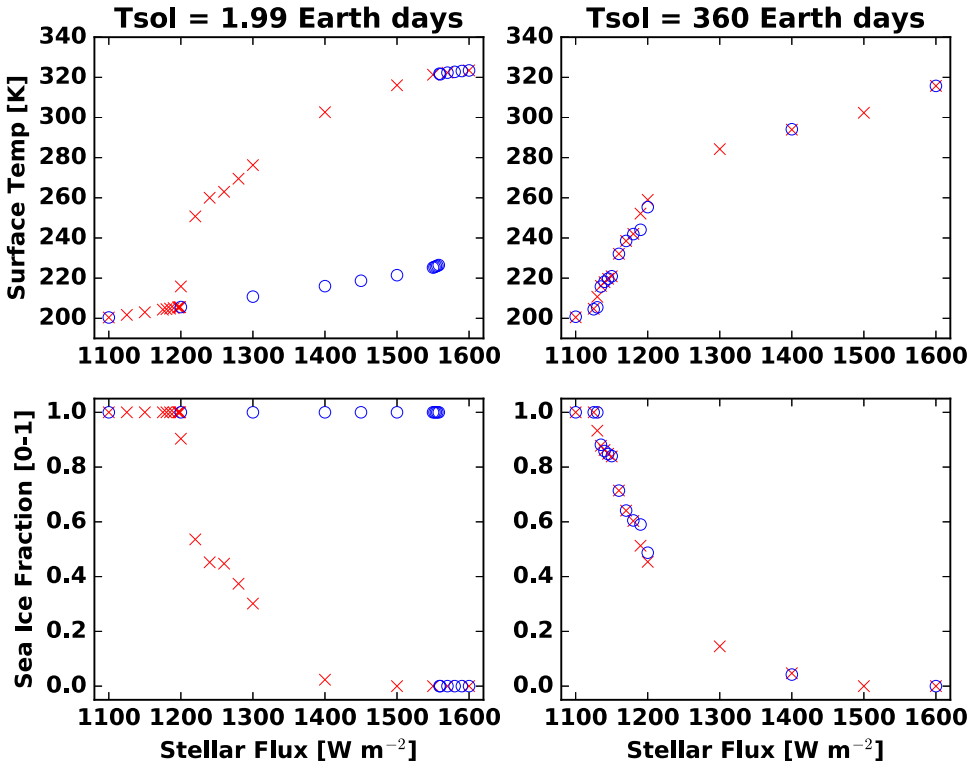


**Figure 2.** Increasing the length of the solar day decreases the hysteresis associated with the snowball bifurcation. This plot shows the equilibrated global mean surface temperature (top) and sea ice fraction (bottom) for simulations with solar days of 1.99 Earth days (left) and 360 Earth days (right) as a function of the stellar flux. Red x's are warm start simulations and blue circles are cold start simulations.

conclude that for a solar day of 360 Earth days, the climate behaves effectively as if the planet were tidally locked.

As the solar day is increased, the amount of hysteresis drops rapidly up to a solar day on the scale of 100 Earth days, and then slowly until hysteresis is completely lost (Figure 3). As noted by Boschi & Lucarini (2013), this loss of hysteresis is accompanied by a general reorientation of the climate from symmetry around the rotational axis (zonal symmetry) for small solar days to something approaching the symmetry seen in synchronously rotating planets (Figure 4). Synchronously rotating planets tend to be roughly symmetric around the stellar flux axis that connects the substellar and anti-stellar points (Pierrehumbert 2011; Koll & Abbot 2015, 2016). Maps of sea ice for simulations with solar days of hundreds of Earth days have a symmetry like this except that it lags the moving substellar point slightly (Figure 4).

The loss of hysteresis as the solar day is increased is mostly associated with a decrease in the stellar flux of the snowball-to-warm transition (Figure 5). Figure 6 shows why the snowball-to-warm transition is strongly affected by the length of the solar day. For longer solar days, the substellar point moves more slowly across the planet's surface, allowing the temperature of the substellar region (at the equator) to increase more (Figure 6). As a result, melting occurs at the substellar point, which decreases the substellar albedo due to melt pond formation, a parameterized process in PlaSim. This leads to a dramatic increase in the stellar radiation absorbed by the surface, which allows the equatorial regions to stay warm throughout the year. As a result, the equatorial ice thins (Figure 6). Once the ice becomes thinner than its seasonal cycle of about 2 m, it melts through to the ocean at the substellar point, engaging strong ice-albedo feedbacks and causing deglaciation from the snowball state.

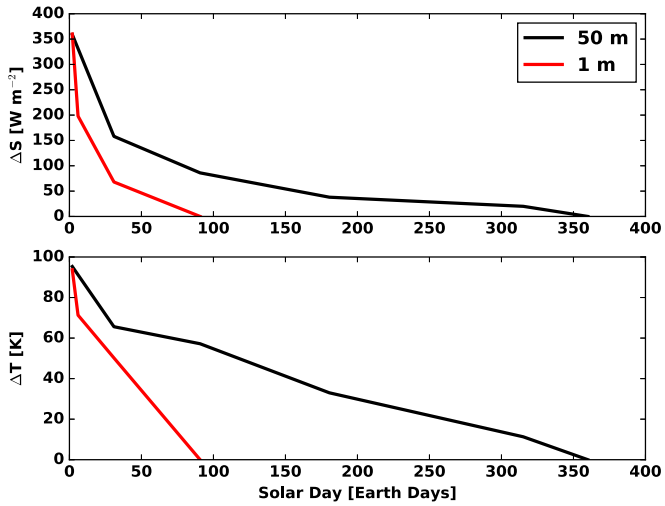


**Figure 3.** This plot shows how the hysteresis and bistability are lost as the solar day is increased. Both the range of stellar flux over which the planet is bistable ($\Delta S$, top) and the increase in global mean surface temperature associated with the snowball-to-warm transition ($\Delta T$, bottom) are shown as a function of the solar day. See Figure 1 for a schematic diagram of $\Delta S$ and $\Delta T$. Results are shown for simulations assuming the slab ocean has a mixed layer depth of 50 m (black) and 1 m (red).

In contrast, the stellar flux of the warm-to-snowball transition is relatively constant as the length of the solar day is increased (Figure 5). As the solar day gets longer, equatorial points experience larger diurnal cycles in surface temperature. This makes the onset of glaciation during the night more likely. For shorter solar days, the planet has a zonal symmetry

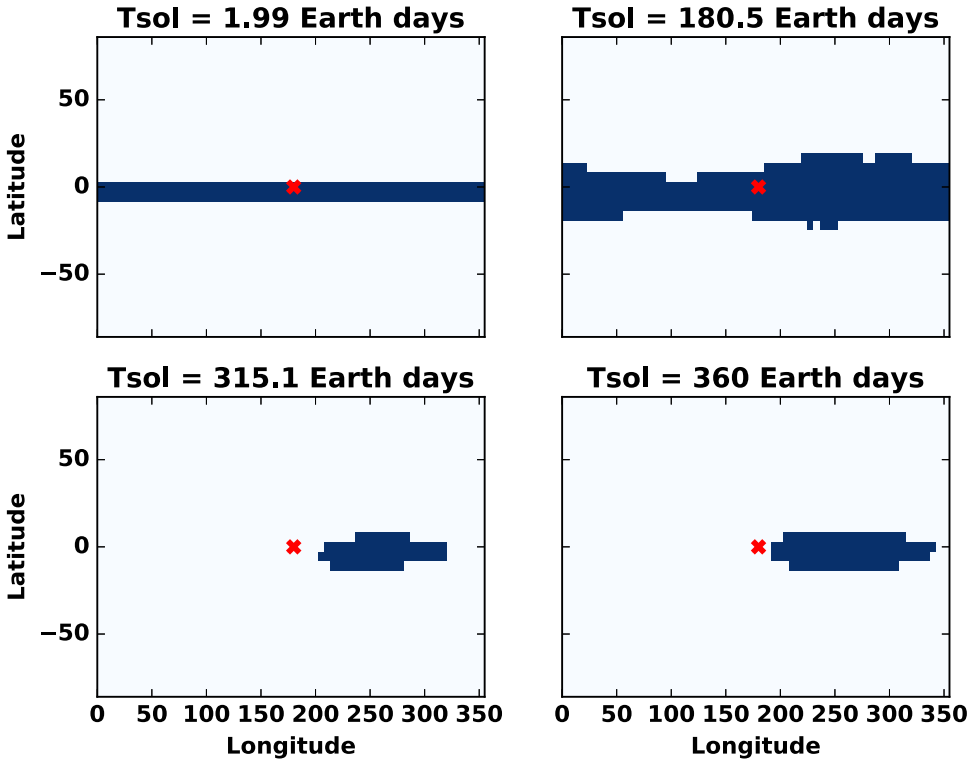


**Figure 4.** As the solar day increases, the axis of symmetry changes. This plot shows maps of the sea ice coverage (very light blue) and open ocean coverage (dark blue) for climate states with a stellar flux just high enough to avoid global ice coverage for a variety of solar days. The red *x* represents the substellar point. For a solar day of 1.99 Earth days, the surface ice pattern of the planet is zonally symmetric and, for a solar day of 360 Earth days, the surface ice pattern of the planet is symmetric around the axis connecting the substellar and anti-stellar points (with a slight eastward offset). For intermediate solar days, the surface ice pattern of the planet transitions between these limits.

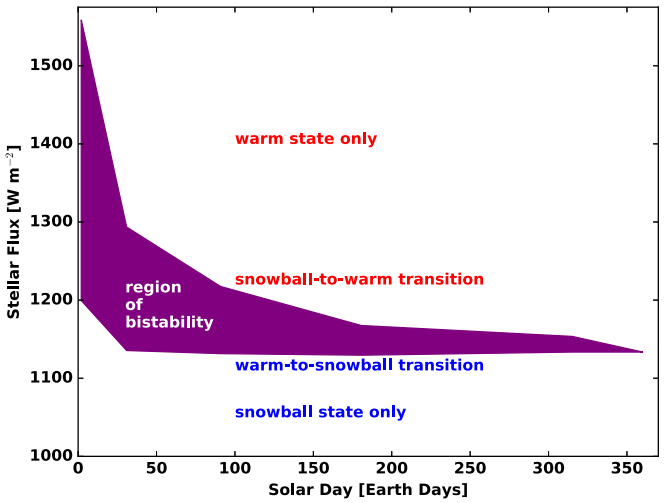


**Figure 5.** This plot shows the stellar flux of the warm-to-snowball transition and the snowball-to-warm transition as a function of the length of the solar day. The region of bistability between the bifurcations is magenta. The warm-to-snowball transition is fairly independent of solar day, but the stellar flux of the snowball-to-warm transition decreases strongly as the solar day increases. A 50 m mixed layer depth is used in these simulations.

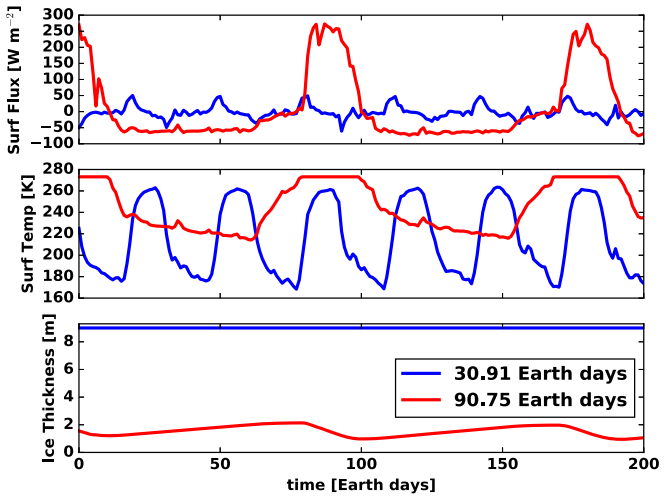


**Figure 6.** This plot shows why increasing the length of the solar day causes the snowball-to-warm transition to occur at a lower stellar flux. The surface heat flux (top), surface temperature (middle), and ice thickness (bottom) for a gridbox at the equator are displayed as a function of time for solar days of 30.91 Earth days (blue) and 90.75 Earth days (red). The stellar flux is 1200 W m$^{-2}$ and the model is in the snowball state in both cases.

(Figure 4), and therefore nighttime glaciation is likely to lead to global glaciation. For longer solar days, the planet can support solutions with ice during the night and open ocean during the day at the equator (Figure 4). These states are often associated with less day-side ice coverage than zonally symmetric states at a similar stellar flux (Salameh et al. 2017). This means that the stellar flux must be decreased more than would otherwise be necessary in order to cause global glaciation for longer solar days. The complex interaction between larger diurnal temperature cycles and changes in planetary symmetry leads to a warm-to-snowball transition that is nearly independent of the length of the solar day in PlaSim, but this result may not be true in all models.

Next we consider how changing the mixed layer depth affects the snowball bifurcations and hysteresis. Using a mixed

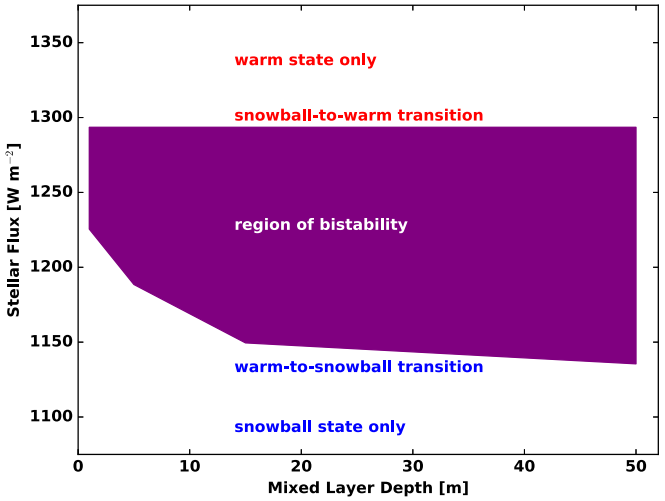


**Figure 7.** This plot shows the stellar flux of the warm-to-snowball transition and the snowball-to-warm transition as a function of the depth of the ocean mixed layer. The region of bistability between the bifurcations is colored magenta. The stellar flux of the snowball-to-warm transition is independent of the mixed layer depth, but the stellar flux of the warm-to-snowball transition decreases as the mixed layer depth increases. The solar day is 30.91 Earth days in these simulations.

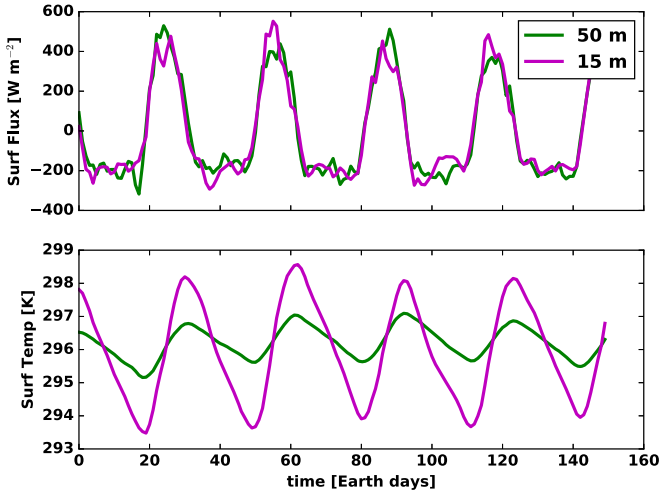


**Figure 8.** This plot shows why increasing the ocean mixed layer depth causes the warm-to-snowball transition to occur at a higher stellar flux. The surface heat flux (top) and surface temperature (bottom) for a gridbox at the equator are displayed as a function of time for mixed layer depths of 50 m (green) and 15 m (magenta). The stellar flux is 1235 W m$^{-2}$, the solar day is 30.91 Earth days, and the model is in the warm state in both cases.

layer depth of 1 m instead of 50 m significantly lowers the length of the solar day at which hysteresis is lost (Figure 3). Changing the mixed layer depth does not affect the snowball-to-warm transition (Figure 7). The ocean is covered with ice when this transition is encountered, so the ocean mixed layer depth does not affect the surface climate. Decreasing the mixed layer depth increases the stellar flux of the warm-to-snowball transition (Figure 7) in a straightforward way. All else being equal, the main effect of decreasing the mixed layer depth is to increase the magnitude of the surface temperature fluctuations along the equator associated with the diurnal cycle in the warm state (Figure 8). This means that for a smaller mixed layer depth the minimum temperature in the cycle will cross the freezing point, initiating the ice-albedo feedback that leads to global glaciation, at a higher stellar flux. Consequently, the stellar flux of the warm-to-snowball transition increases.

## 4. Discussion

Checlair et al. (2017) raised the question of how close a planet needs to be to synchronous rotation in order to lose the snowball bifurcations and climate hysteresis. Our results (Section 3) indicate that even slight increases in the solar day (Figure 3) significantly reduce climate hysteresis, but the solar day needs to be hundreds of Earth days in order to completely remove hysteresis. Leconte et al. (2015) showed that planets in a circular orbit can get caught in spin states with roughly two rotations per orbit. This means that their solar day would be roughly equal to their orbital period (Section 2.2). Using the scalings in Kopparapu et al. (2016), a planet that received the same stellar flux as Earth would have an orbital period of 65 Earth days for a stellar mass of 50% of the Sun's. Our results suggest that a planet with a solar day of 65 Earth days and a mixed layer depth of 50 m would have hysteresis over about one-third of the range of stellar flux as modern Earth, and with a mixed layer depth of 1 m it would have nearly completely lost hysteresis. If the stellar mass was 80% of the Sun's a similar planet would have a solar day of 209 Earth days, making the reduction in hysteresis larger. Furthermore, these reductions in hysteresis would be even more dramatic if the reduction in the ice albedo due to the spectrum of a redder star were accounted for (Joshi & Haberle 2012; Shields et al. 2013, 2014).

This study represents an idealized investigation of the physical mechanisms through which climate hysteresis is lost as the solar day increases. For theoretical clarity, we have purposefully isolated changes in the solar day, while keeping other variables constant. To apply these results to observed planets it will be necessary to perform simulations using the best observational estimates of the stellar spectrum, orbital distance, orbital period, eccentricity, planetary rotation rate, planetary size, atmospheric mass, and all other relevant variables. Accurately accounting for each of these variables can effect the results, as Kopparapu et al. (2016) showed when they revisited the more idealized paper of Yang et al. (2013).

In this study, we have not included ocean and thick ice dynamics. One important aspect of ocean circulation is that on the night side of a planet with a deep ocean, convection would be likely, extending the mixed layer all the way to the bottom of the ocean. This would tend to reduce the surface temperature drop experienced on the night side, and delay the warm-to-snowball transition. Efficient flow of thick ice from higher latitudes toward the equator (Goodman & Pierrehumbert 2003; Pollard & Kasting 2005; Goodman 2006; Li & Pierrehumbert 2011; Tziperman et al. 2012; Abbot et al. 2013; Pollard et al. 2017) would tend to thicken the ice there, despite the mechanism described in Section 3. This would lessen the reduction in the stellar flux of the snowball-to-warm transition as the length of the solar day is increased. Both of these effects would tend to make the hysteresis experienced by a planet larger than what we have estimated here. Work with models including ocean dynamics and flowing thick ice is required to determine the importance of these issues.

Many planets in the habitable zone with low $CO_2$ outgassing rates may experience continuous cycling between warm and snowball conditions, rather than equilibrating in the warm state (Tajika 2007; Kadoya & Tajika 2014; Menou 2015; Abbot 2016; Batalha et al. 2016; Haqq-Misra et al. 2016; Paradise &

Menou 2017). The amount of time spent in the snowball state, which represents the majority of the period of the cycles, is proportional to the $CO_2$ needed to cause deglaciation if we assume a constant $CO_2$ outgassing flux (Abbot 2016). Since increasing the solar day decreases the amount of forcing necessary to cause snowball deglaciation (Figure 7), this means that planets with long solar days and low $CO_2$ outgassing rates would experience much more rapid cycles between the warm and snowball climate states. That said, planets orbiting M and K stars are less likely to experience climate cycles at all due to the reduced ice-ocean albedo contrast (Haqq-Misra et al. 2016).

We have not taken into account the implications of $CO_2$ condensation (Turbet et al. 2017) in the snowball state in this paper. Since the surface temperature can drop below 195 K, the sublimation point of $CO_2$ at a surface pressure of 1 bar, even at the equator in the snowball state (Figure 6), this is an issue that warrants further investigation. $CO_2$ condensation would not significantly affect the calculations we have made since we assumed a low atmospheric $CO_2$ concentration and varied the stellar flux. It could, however, be important in a snowball scenario involving the carbon cycle and variations in $CO_2$ (Walker et al. 1981; Kirschvink 1992; Hoffman et al. 1998). The slow-moving location of the substellar point and large diurnal temperature variations, which would force $CO_2$ sublimation and condensation, would make this problem particularly interesting.

The thermodynamic sea ice scheme in the model uses a 0D Semtner formulation (Semtner 1976). This means there are no interior levels in the ice, and that the temperature profile within the ice is assumed to be linear between the melting point at the bottom and the surface temperature at the top. This approximation will yield reasonable heat fluxes through the ice and surface temperatures as long as the ice is thinner than a few multiples of the critical thickness, $z^* = \sqrt{\frac{\kappa P}{\pi}}$, where $P$ is the period of variations in surface forcing (the solar day) and $\kappa \approx 10^{-6}\,\mathrm{m^2\ s^{-1}}$ is the thermal diffusivity of ice (Abbot et al. 2010). For $P = 30$ Earth days, $z^* = 0.9$ m and for $P = 90$ Earth days, $z^* = 1.6$ m. This means that the sea ice model should be providing a reasonable approximation of surface temperature (and melting) near the equator when the ice is thin enough (less than about 2 m) to lead to deglaciation from the snowball state for most of the solar days considered here (Figure 6). Nevertheless, it might still be interesting to investigate these processes using a more sophisticated sea ice model.

A planet with an obliquity of 90° would experience variations in stellar flux that are somewhat similar to a planet caught in a 2:1 spin–orbit resonance. Our results suggest that such a planet might experience reduced hysteresis in planetary climate if its orbital period is tens to hundreds of days. Calculations by Kilic et al. (2017) using a similar modeling framework show that this is indeed the case, especially when the warm state is defined as any state with at least some open ocean, as we have done here.

## 5. Conclusions

We have used PlaSIM, an intermediate complexity global climate model run with a mixed layer ocean and no ocean heat transport, to investigate the snowball bifurcations and hysteresis in planetary climate as a function of the length of the solar day. Our main conclusions are as follows:

1. Hysteresis in planetary climate (the range in stellar flux for which there is bistability) is significantly reduced if the solar day is increased to tens of Earth days. This effect is stronger the smaller the mixed layer depth is. This would be relevant to any tidally influenced, but not synchronously rotating, planet orbiting an M or K star.
2. Hysteresis in planetary climate is lost and the planet transitions smoothly into a snowball state if the solar day is increased to hundreds of Earth days. This could be relevant to tidally influenced planets orbiting late M and K stars.
3. Increasing the length of the solar day mainly decreases hysteresis in planetary climate by decreasing the stellar flux of the snowball-to-warm transition. This happens because the substellar point is heated for longer if the solar day is longer, leading to melting and a reduction in albedo there, which leads to a higher mean surface temperature throughout the day and thinner ice. Once the ice is thin enough, it melts through to the ocean at its diurnal minimum, kicking off a large-scale ice-albedo feedback that leads to total deglaciation.
4. Decreasing the depth of the ocean mixed layer mainly decreases hysteresis in planetary climate by increasing the stellar flux of the warm-to-snowball transition. This is because all else being equal, a smaller mixed layer depth causes larger fluctuations in ocean surface temperature. This means that the diurnal minimum in equatorial surface temperature is more likely to cross the freezing point, leading to ice formation and a large-scale ice-albedo feedback that leads to complete glaciation.

We thank R. Boschi for sharing and explaining his modifications to the PlaSim radiation code and T. Komacek for comments on an early draft of this paper. We acknowledge support from the NASA Astrobiology Institutes Virtual Planetary Laboratory, which is supported by NASA under cooperative agreement NNH05ZDA001C. We acknowledge support from NASA grant number NNX16AR85G, which is part of the "Habitable Worlds" program. We acknowledge support from the National Science Foundation under NSF award number 1623064. P.P. was supported by a NASA Earth and Space Science Fellowship.

## ORCID iDs

Dorian S. Abbot https://orcid.org/0000-0001-8335-6560

## References

Abbot, D. S. 2016, ApJ, 827, 117
Abbot, D. S., Eisenman, I., & Pierrehumbert, R. T. 2010, JCli, 23, 6100
Abbot, D. S., & Pierrehumbert, R. T. 2010, JGR, 115, D03104
Abbot, D. S., Voigt, A., Branson, M., et al. 2012, GeoRL, 39, L20711
Abbot, D. S., Voigt, A., & Koll, D. 2011, JGR, 116, D18103
Abbot, D. S., Voigt, A., Li, D., et al. 2013, JGR, 118, 6017
Barnes, R. 2016, CeMDA, 129, 509
Batalha, N. E., Kopparapu, R. K., Haqq-Misra, J., & Kasting, J. F. 2016, E&PSL, 455, 7
Boschi, R., & Lucarini, V. 2013, EPSC, 2013, 832
Budyko, M. I. 1969, Tell, 21, 611
Checlair, J., Menou, K., & Abbot, D. S. 2017, ApJ, 845, 132
Cullum, J., Stevens, D. P., & Joshi, M. M. 2016, PNAS, 113, 4278
Fraedrich, K., Jansen, H., Kirk, E., Luksch, U., & Lunkeit, F. 2005, MetZe, 14, 299
Goodman, J. C. 2006, GeoRL, 33, L16701
Goodman, J. C., & Pierrehumbert, R. T. 2003, JGRC, 108, 3308

Haqq-Misra, J., Kopparapu, R. K., Batalha, N. E., Harman, C. E., & Kasting, J. F. 2016, ApJ, 827, 120
Haqq-Misra, J., Wolf, E., Joshi, M., et al. 2017, arXiv:1710.00435
Hoffman, P. F., Kaufman, A. J., Halverson, G. P., & Schrag, D. P. 1998, Sci, 281, 1342
Hoffman, P. F., & Schrag, D. P. 2002, TeNov, 14, 129
Hu, Y., & Yang, J. 2014, PNAS, 111, 629
Joshi, M. M., & Haberle, R. M. 2012, AsBio, 12, 3
Kadoya, S., & Tajika, E. 2014, ApJ, 790, 107
Kasting, J. F., Whitmire, D. P., & Reynolds, R. T. 1993, Icar, 101, 108
Kilic, C., Raible, C. C., & Stocker, T. F. 2017, ApJ, 844, 147
Kirschvink, J. 1992, in The Proterozoic Biosphere: A Multidisciplinary Study, ed. J. Schopf & C. Klein (New York: Cambridge Univ. Press), 51
Koll, D. D. B., & Abbot, D. S. 2015, ApJ, 802, 21
Koll, D. D. B., & Abbot, D. S. 2016, ApJ, 825, 99
Kopparapu, R. K., Wolf, E. T., Haqq-Misra, J., et al. 2016, ApJ, 819, 84
Laakso, T. A., & Schrag, D. P. 2014, E&PSL, 388, 81
Laakso, T. A., & Schrag, D. P. 2017, Geobiology, 15, 366
Leconte, J., Forget, F., Charnay, B., et al. 2013b, A&A, 554, A69
Leconte, J., Forget, F., Charnay, B., Wordsworth, R., & Pottier, A. 2013a, Natur, 504, 268
Leconte, J., Wu, H., Menou, K., & Murray, N. 2015, Sci, 347, 632
Li, D., & Pierrehumbert, R. T. 2011, GeoRL, 38, L17501
Lucarini, V., Pascale, S., Boschi, R., Kirk, E., & Iro, N. 2013, AN, 334 576
Menou, K. 2015, E&PSL, 429, 20
Paradise, A., & Menou, K. 2017, ApJ, 848, 33
Pierrehumbert, R. T. 2011, ApJL, 726, L8
Pollard, D., & Kasting, J. F. 2005, JGRC, 110, C07010
Pollard, D., Kasting, J. F., & Zugger, M. E. 2017, JGRD, 122, 5157
Rooney, A. D., Strauss, J. V., Brandon, A. D., & Macdonald, F. A. 2015, Geo, 43, 459
Rose, B. E. 2015, JGRD, 120, 1404
Salameh, J., Popp, M., & Marotzke, J. 2017, ClDy, 1
Sellers, W. D. 1969, JApMe, 8, 392
Semtner, A. J. 1976, JPO, 6, 379
Shields, A. L., Bitz, C. M., Meadows, V. S., Joshi, M. M., & Robinson, T. D. 2014, ApJL, 785, L9
Shields, A. L., Meadows, V. S., Bitz, C. M., Pierrehumbert, R. T., Joshi, M. M., & Robinson, T. D. 2013, AsBio, 13, 715
Tajika, E. 2007, EP&S, 59, 293
Turbet, M., Forget, F., Leconte, J., Charnay, B., & Tobie, G. 2017, E&PSL, 11, 11
Tziperman, E., Abbot, D. S., Ashkenazy, Y., et al. 2012, JGR, 117, C05016
Voigt, A. 2013, ESDD, 4, 927
Voigt, A., & Abbot, D. S. 2012, CliPa, 8, 2079
Voigt, A., Abbot, D. S., Pierrehumbert, R. T., & Marotzke, J. 2011, CliPa, 7, 249
Voigt, A., Held, I. M., & Marotzke, J. 2012, JAtS, 69, 116
Walker, J. C. G., Hays, P. B., & Kasting, J. F. 1981, JGR, 86, 9776
Way, M., Del Genio, A., Kelley, M., Aleinov, I., & Clune, T. 2015, arXiv:1511.07283
Wolf, E., & Toon, O. 2014, GeoRL, 41, 167
Wolf, E., & Toon, O. 2015, JGR, 120, 5775
Wolf, E. T. 2017, ApJL, 839, L1
Wolf, E. T., Shields, A. L., Kopparapu, R. K., Haqq-Misra, J., & Toon, O. B. 2017, ApJ, 837, 107
Yang, J., Boué, G., Fabrycky, D. C., & Abbot, D. S. 2014, ApJL, 787, L2
Yang, J., Cowan, N. B., & Abbot, D. S. 2013, ApJL, 771, L45
Yang, J., Peltier, W., & Hu, Y. 2012a, JCli, 25, 2711
Yang, J., Peltier, W., & Hu, Y. 2012b, JCli, 25, 2737
Yang, J., Peltier, W. R., & Hu, Y. 2012c, CliPa, 8, 907